International Journal of Control, Automation and Systems 19(10) (2021) 3522-3532
http://dx.doi.org/10.1007/s12555-019-1058-5
ISSN:1598-6446 eISSN:2005-4092
http://www.springer.com/12555

EMG Based Control of Transhumeral Prosthesis Using Machine Learning Algorithms

Neelum Yousaf Sattar*, Zareena Kausar, Syed Ali Usama, Umer Farooq, and Umar Shahbaz Khan

Abstract: This research presents work on control of a prosthetic arm using surface electromyography (sEMG) signals acquired from triceps and biceps of fifteen healthy and four amputated subjects. Myo armband was used to acquire sEMG signals corresponding to four different arm motions: elbow extension, elbow flexion, wrist pronation, and wrist supination. Ten time-domain features were extracted and considered for classification to recognize the four-arm motions. These features and their various combinations were used to train four different classifiers, in both offline and real-time settings. It was found that the combination of signal mean and waveform length as a feature and k-nearest neighbors as classifier performed significantly better ($p < 0.05$) than all other combinations in both offline and real-time settings. The offline accuracies of 95.8% and 68.1% and real-time accuracies of 91.9% and 60.1% were obtained for healthy and amputated subjects, respectively. Results obtained using the presented scheme successfully demonstrate that using suitable features and classifier, classification accuracies can be significantly improved for transhumeral prosthesis, thereby, providing better, wearable and non-invasive control of prostheses using sEMG signals.

Keywords: *k*-nearest neighbors, myo armband, prosthetic arm, real-time classification, surface electromyography, transhumeral amputation.

1. INTRODUCTION

People suffering from amputation and disability have difficulties using old rehabilitation devices, therefore, there is a need to develop more innovative human-machine interfaces (HMI) for active prosthesis [1]. The active prosthetic device is the one which mimics natural human limb motion by providing external power through motors to perform greater functionality however, they also represent the system with the highest complexity. HMI relies on sensors to detect motions and control the prosthetic device. Although several prosthetic devices with biosignals as a control source are developed for below-elbow amputation [2], while in literature limited work is done on prostheses for higher amputation [3]. It is because there are higher DOF (degrees-of-freedom) to be controlled but fewer residual upper limb muscles available for biosignals.

Two major types of an active upper-limb prosthesis for transhumeral amputation are i) body-powered prosthesis and ii) myoelectric prosthesis [4]. In body-powered prosthesis, a harness allows the amputated person to actuate the prosthetic device by executing some specific shoulder motions. Whereas in a myoelectric prosthesis, the prosthetic arm is controlled with the electrical signals generated as a result of the movement of the remaining muscles present on an arm. The obtained signal is sent to the controller, which analyzes and processes the obtained information, causes the prosthetic arm to move.

Over the years, researchers have used different biosensors such as surface electromyogram (sEMG), intramuscular EMG (iEMG) force myography (FMG), inertial measurement unit (IMU), functional near-infrared spectroscopy (fNIRS) [5,6], electroencephalogram (EEG), mechanomyogram (MMG) and electrooculography (EOG) to control human upper limb prosthese [1,7,8]. sEMG signal recorded from the residual upper limb muscles of amputees is a significant source of control input for powered upper-limb prosthetic devices to restore limb functionality [9]. As EMG comprises of motor information from which limb motion intention could be identified, this information can be retained from residual muscles of an amputee as well. EMG signals can be obtained by both invasive and non-invasive procedures. iEMG electrodes are used for invasive techniques whereas sEMG electrodes are employed for a non-invasive solution. Ear-

Manuscript received December 19, 2019; revised May 9, 2020, May 11, 2020, September 23, 2020, and January 4, 2021; accepted January 11, 2021. Recommended by Associate Editor Noman Naseer under the direction of Editor-in-Chief Keum-Shik Hong.

Neelum Yousaf Sattar, Zareena Kausar, Syed Ali Usama, and Umer Farooq are with the Department of Mechatronics and Biomedical Engineering, Air University, Islamabad, Pakistan (e-mails: neelumyousafsattar@gmail.com, zareena.kausar@mail.au.edu.pk, ali.usama@mail.au.edu.pk, maill2umer@gmail.com). Umar Shahbaz Khan is with the Department of Mechatronics Engineering, CEME, National University of Sciences and Technology, Islamabad, Pakistan (e-mail: u.shahbaz@ceme.nust.edu.pk).
* Corresponding author.

lier studies have reported similar classification accuracy for multiple classes of arm movements using iEMG and sEMG electrodes [10]. The signals are fed to filters for pre-processing [11]. Therefore, sEMG remains the most feasible clinical option for acquiring EMG signals from upper-limb mostly because it is non-invasive and could still offer related performance with iEMG. An EMG-based HMI, that can be easily used in daily life, should be simple, non-invasive and wearable.

With the advancements in wearable sensors technologies, sEMG data can also now be acquired using wearable armbands. These armbands usually include multiple EMG sensors that are positioned radially around the circumference of a flexible band, allowing ease of wearing. Arguably the most widely used sEMG armband is Myo armband by Thalmic Labs. It is a low-cost consumer-grade EMG device that integrates an ARM Cortex-M4-based microcontroller unit and a set of eight dry EMG electrodes.its application is not limited to prosthesis alone, it has been used for: formation control using interpreters, stroke rehabilitation [12], physiotherapy training, and several other applications. The biggest challenge, however, is to gather helpful data from raw electromyographic signals to detect human muscle intention and generate a control command for the transhumeral prosthesis [13]. For this study, sEMG signals acquired from Myo armband are processed in the subsequent steps: signal feature extraction, signal classification, and to generate control commands for arm movement. The feature extraction technique is used to gather useful information for classification of sEMG signals [14]. Then, the extracted features and their different combinations are classified through machine learning classifiers. Ultimately, the trained classifier is used for control commands generation of arm movements [23].

Numerous preceding studies have successfully shown the feasibility of using pattern recognition algorithms to classify upper limb motions [1,15,16]. However, very few of them have applied these pattern recognition algorithms to control a prosthetic arm fixed on transhumeral amputees [3,17], indicating a significant weakness as its is a fact that the obtained sEMG signals from the remaining limb are different from the signals gather from a healthy subject limb [18]. This is because, in most of the upper extremity amputations, there are not enough muscles present that could be easily used by the amputees. Pullian *et al*. evaluated the feasibility of predicting dynamic arm movements (both flexion/extension and pronation/supination) based on iEMG signals using Optotrak Certus motion capture system (Northern Digital Inc; Waterloo, Canada intramuscular electrodes for five transhumeral subjects [19]. An offline training of Artificial Neural Network was performed to anticipate arm trajectory of sEMG signals. In another study, Pasquina *et al*. demonstrated that implantable myoelectric sensors can be used for wireless transmission of EMG signals and they aid in capturing complex human hand motions too [20]. Geethanjali added that only soft computing or offline signal processing techniques are currently addressed and very fewer studies reflect hardware systems and hence there exist a need for real-time implementation of these soft computing techniques [21]. Fifer *et al*. objective was to obtain simultaneous neural control of reach and grasp movement of a dexterous prosthetic arm developed at Johns Hopkins University. [22]. The achieved classification accuracy for reach and grasp movements was about to 86%. Bandara *et al*. proposed to use EEG signals for motion intention prediction of two major upper limb functions: arm lifting and the hand reaching. Four different features provided input to the neural network and kNN based classifiers and claimed to achieve maximum accuracy of 72.5% [23]. In another research, Sittiwanchai *et al*. presented a 3D printed prototype of a transhumeral prosthetic arm and its elbow joint control through sEMG. Signals were acquired from individual biceps and triceps using sEMG sensors ID2PADW produced by Oisaka Electronic Equipment Ltd [24]. A rotation speed command was generated for the servomotors based on the extracted feature values to identify and separate muscle contraction and relaxation. It is evident from literature, the performance of multiple transradial prosthetic arms have been tested using Myo armband but certainly, no non-invaisve solution using Myo armband has been presented previously to control a transhumeral prosthetic arm [25].

For this research, we seek to estimate the achieved accuracy of different sEMG features and classification algorithms for transhumeral prosthesis. The authors focus is on the effectiveness of the selected features and classifiers for transhumeral amputees, as the populace of transhumeral amputee institutes approximately one-third of the total upper extremity amputation. This will develop a recommendation for the utility of the selected features and algorithm in the useful manoeuvring of a myoelectric transhumeral prosthesis. sEMG signal acquisition and processing were done for four different arm motions: Elbow Extension (EE), Elbow Flexion (EF), Wrist Pronation (WP) and Wrist Supination (WS) using Myo armband. Fifteen healthy and four amputated subjects participated in this study. Four different classifiers, namely LDA, SVM, quadratic discriminant analysis (QDA) and k-nearest neighbors (kNN), were analyzed for the acquisition of maximum classification accuracies. Furthermore, three real-time performance parameters: selection time (ST), completion time (CT) and real-time accuracy (RA) were adopted to quantify and compare the performance of classifiers. A 3D printed transhumeral prosthetic arm prototype was tested for real-time analysis and it was able to control 2 DOF to provide elbow flexion-extension and wrist supination-pronation. For offline setting, among all the features combination of signal mean and wavelength

Table 1. Demographic characteristics of four amputees.

Patient ID	A1	A2	A3	A4
Gender	Male	Male	Male	Male
Age	23	27	32	45
Amputated side	Right	Left	Right	Right
Residual length	15 cm	17 cm	10cm	18cm
Cause of amputation	Accident	Accident	Accident	Diabetes

features performed the best and kNN showed greater statistical significance ($p < 0.05$) in comparison with other machine learning classifiers. The experimental outcomes are presented to exhibit the usefulness and outcome performance of proposed research with obtained classification accuracy, features and their different combinations for different arm motions. The proposed scheme has provided a user-friendly and non-invasive solution to enhance the real-time accuracy of the prosthetic arm for transhumeral amputees.

2. SIGNAL ACQUISITION AND PROCESSING

2.1. Subject information and experimental protocol

Fifteen healthy subjects (aged 20∼35, denoted as S1∼S15) and four transhumeral amputees were recruited for this study; the demographic characteristics of the four amputees (denoted as A1, A2, A3 and A4) are given in Table 1. Air University Human Research Ethics Committee (AUHREC) approved the study. All subjects were informed about the experimental procedure in detail, and they provided their written consent before the start of experiments. Prior to commence of experiments, all the subjects were requested have an initial 10 s rest followed by a 80s task period [26,27]. This task period consisted of the four arm motions, EE, EF, WP and WS. Each repeated seven times at a self-paced frequency of approximately 1 Hz. This experiment was performed on all fifteen healthy subjects right arms and four amputees. A healthy subject is shown in Fig. 1(a). during experiment. Detailed experimental paradigm is illustrated in Fig. 1(b).

2.2. Signal acquisition

Myo armband by Thalmic Labs was used to acquire sEMG signals. It is a wearable and resizable device which allows the freedom to acquire sEMG signals from different arm sizes (thin or thick). It includes eight sEMG sensors and a 9-axis inertial measurement unit which have an accelerometer, a magnetometer, and a gyroscope with all having three axes. The Myo armband has a sampling frequency of 200 Hz.

sEMG signal strength is affected by different muscle positions, such as for sitting or standing, and human body

(a)

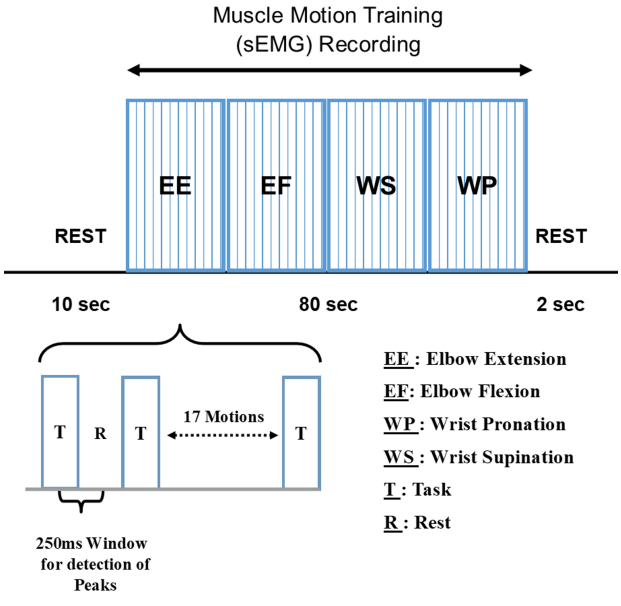

(b)

Fig. 1. (a) Myo armband placed on the bicep of a healthy and amputee subject's right arm to acquire EMG signals, and calibration of four different motions including EE, EF, WP and WS. (b) Experimental paradigm.

temperature. Myo armband was placed on the biceps of the subjects while they were standing. After sensor placement, the Myo armband was connected to a laptop via

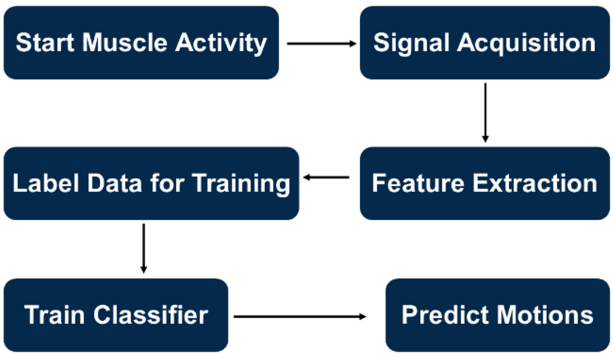

Fig. 2. Flow diagram of sEMG signal acquisition and processing.

a USB Bluetooth adapter. Myo diagnostics software was used to display signals in graphical form for each electrode. The signals on this graphical display can be visually inspected to see which electrodes are active during a specific task. The signals were captured during the experiments using the Myo Capture tool of the software. Myo Capture stored the time-series of all the numerical values of voltages obtained from the sensors, in an auto-generated Microsoft excel® sheet. This excel sheet contained nine columns, eight containing data for eight electrodes and one containing time points. Fig. 2 represents flow diagram of sEMG signal acquistion and processing.

2.3. Signal processing

The armband has an integrated operational amplifier for sEMG signal amplification within the sEMG electrodes. Myo armband extracts data as an analog voltage in millivolts (mV) and uses its built-in filters to remove noise(s) and yields a noise-free 8-bit data [28]. The output voltages vary between -30 mV to +80 mV. These voltages are digitized in the range from -128 to 127 and later normalized between -1 and +1 for data processing in MATLAB®. Fig. 3 shows the averaged raw signal obtained from eight electrodes of the armband for each arm motion.

3. FEATURE EXTRACTION

The process of feature extraction plays a vital role in defining the discriminatory information carried by signals. Based on this information, the signals are differentiated from each other [5,29]. In this study, ten different features namely signal mean (SM), variance (σ), skewness (SSK), kurtosis (SK), slope (SS), waveform length (WL), mean absolute value (MAV), root mean square (RMS), Willison amplitude (WAMP), and Zero Crossing (ZC), were calculated. These features were calculated from only selected electrodes that showed significant activation using 250ms window. Table 2 shows the significantly activated electrodes for each motion.

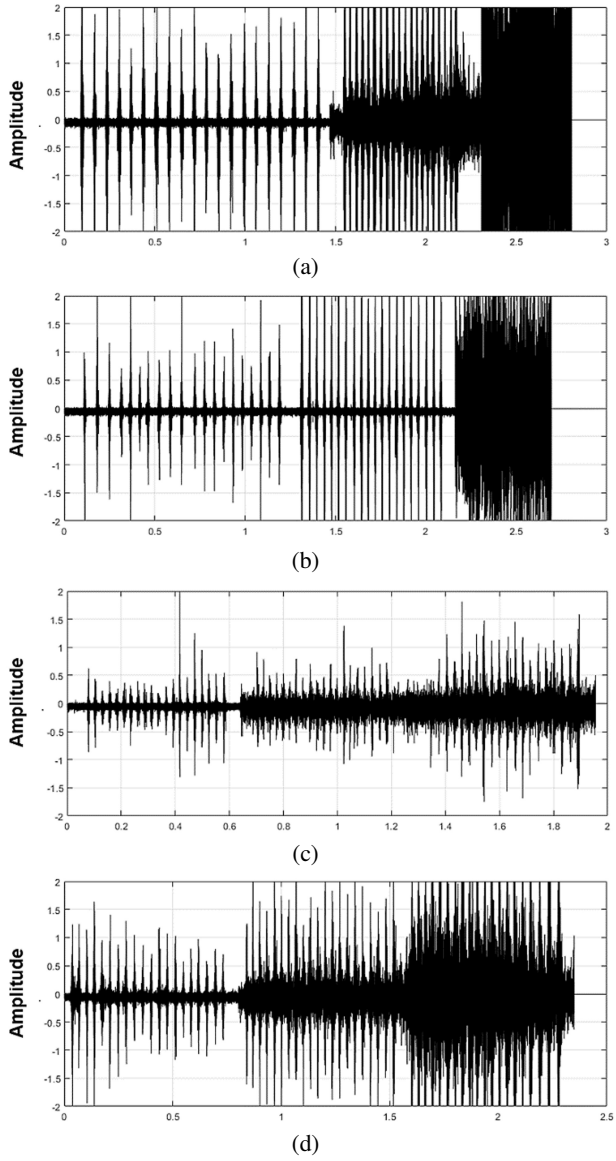

Fig. 3. Extracted raw sEMG signal of a healthy subject through Myo armband: (a) EE (b) EF (c) WP and (d) WS.

Table 2. Activated electrodes of Myo armband.

Electrodes	EE	EF	WS	WP
1	✓		✓	✓
2	✓		✓	
3	✓	✓	✓	
4	✓			
5				✓
6		✓	✓	
7	✓	✓		✓
8		✓	✓	

To ensure activation, the threshold value was set to 55 at an offset of 10 values. This value was selected because it was observed that during the rest positions, the values obtained were in the ranges of 40∼45. The details of each extracted feature are given below:

SM was calculated as (1).

$$\mathrm{SM} = \frac{1}{\mathrm{N}} \sum_{\mathrm{i}=1}^{\mathrm{N}} \mathrm{X_i}, \tag{1}$$

where N denotes the length of the data points within a segment and X_i represents the EMG signal values. SV is the mean value of the square of the deviation of the EMG signal values at variable. It can be calculated by (2).

$$\mathrm{SV} = \frac{1}{\mathrm{N}-1} \sum_{\mathrm{i}=1}^{\mathrm{N}} \mathrm{X_i^2}. \tag{2}$$

SSK is defined as a measure of the asymmetry of obtained signal around its mean. It can be a positive or negative value and was computed as (3).

$$\mathrm{SSK} = \mathrm{E}\left[\left(\frac{\mathrm{X}-\mu}{\sigma}\right)^3\right], \tag{3}$$

where σ is the standard deviation of X and E is the expected value of X.

SK describes the shape of a distribution's tail relative to its complete shape. Mathematically, it is given in (4).

$$\mathrm{SK} = \mathrm{E}\left[\left(\frac{\mathrm{X}-\mu}{\sigma}\right)^4\right]. \tag{4}$$

SS was calculated using the polyfit function in MATLAB® which fits a line to all data points within a segment.

MAV was found by taking the average of the absolute value of the EMG signal. It is usually used for detection of muscle contraction and calculated as in (5).

$$\mathrm{MAV} = \frac{1}{\mathrm{N}} \sum_{\mathrm{i}=1}^{\mathrm{N}} |\mathrm{X_i}|. \tag{5}$$

WAMP is defined by the change in EMG signals amplitude among two adjacent segments which surpasses a predefined threshold to reduce noise. It is given by (6).

$$\mathrm{WAMP} = \sum_{\mathrm{i}=1}^{\mathrm{N}} \mathrm{f}(|\mathrm{X_i} - \mathrm{X_{i+1}}|), \tag{6}$$

whereas

$$f(x) = \begin{cases} 1, & \text{if } x \geq \text{threshold}, \\ 0, & \text{otherwise}. \end{cases}$$

WL is a cumulative variation that represents the variation of EMG signals. It is given by (7).

$$\mathrm{WL} = \sum_{\mathrm{i}=1}^{\mathrm{N}} (|\mathrm{X_i} - \mathrm{X_{i+1}}|). \tag{7}$$

ZC is the number of times the amplitude value of the EMG signal crosses the zero y-axis. As mentioned the threshold value previously for signal activation was set to 55. ZC can be formulated as (8).

$$\mathrm{ZC} = \sum_{\mathrm{i}=1}^{\mathrm{N}} [\mathrm{sgn}(\mathrm{X_i} \times \mathrm{X_{i+1}}) \cap |\mathrm{X_i} - \mathrm{X_{i+1}}| \geq \text{threshold}]. \tag{8}$$

RMS, also known as the quadratic mean, is closely related to the standard deviation as both are equal when the mean of the signal is zero. it can be expressed as (9).

$$\mathrm{RMS} = \sqrt{\frac{1}{\mathrm{N}} \sum_{\mathrm{i}=1}^{\mathrm{N}} \mathrm{X_i^2}}. \tag{9}$$

Different combinations of above-mentioned features were also used for classification. It will be shown in the next section that how appropriate selection of features greatly affects the classification performance.

4. CLASSIFICATION

To comprehensively evaluate the performance of features and their combinations, four widely used classifiers in EMG pattern recognition were employed namely, LDA, SVM, QDA, and kNN.

4.1. LDA

It is on of the most commonly used classifier in machine learning for both online and offline applications. In LDA, all the data points are projected on a line in a way that each class can be separated smoothly. it also decreases the intra- class variance and tend to increase the inter-class mean. This techniques helps to separate different class from each other, and which brings their data points closer to each other so they wont mix with other classes data points [30–33]. LDA algorithm maximizes the Fisher's criterion given in (10).

$$\mathrm{J(v)} = \frac{\mathrm{v^t S_B v}}{\mathrm{v^t S_w v}}. \tag{10}$$

Between classes scatter matrix S_B is defined as (11).

$$\mathrm{S_B} = \sum_{\mathrm{x_i}}^{\mathrm{c}} \mathrm{n_i} (\mu_\mathrm{i} - \mu) (\mu_\mathrm{i} - \mu)^\mathrm{t}, \tag{11}$$

where n_i represents several samples that belong to class i, within class scatter matrix S_w is represented as in (12).

$$\mathrm{S_w} = \sum_{\mathrm{x_i}}^{\mathrm{c}} \mathrm{S_i} = \sum_{\mathrm{x_i}}^{\mathrm{c}} \sum_{\mathrm{x_k} \in \mathrm{Classi}} (\mathrm{x_k} - \mu_\mathrm{i}) (\mathrm{x_k} - \mu_\mathrm{i})^\mathrm{t}. \tag{12}$$

Generalized eigenvector problem can be represented as in (13).

$$\mathrm{S_B v} = \lambda \mathrm{S_w v}. \tag{13}$$

The optimal v is the eigenvector corresponding to the largest eigenvalue can be represented as in (14).

$$v = S_W^{-1}(\mu_i - \mu), \tag{14}$$

provided that S_w is nonsingular.

10-fold cross-validation was performed to estimate LDA classifier performance. It means that the entire data was mixed randomly into ten groups, out of which nine were used for training and one was used for testing. This process was repeated ten times until all groups were tested against each other.

4.2. SVM

It is commonly used to control prosthetic and rehabilitation devices. It usually constructs a hyperplane or set of hyperplanes in a high dimensional space, which is used for classification, regression, or outliers detection [34]. The hyperplanes maximize the margins between different classes which help to accomplish high classification accuracy. Intuitively, a good separation is achieved by the hyperplane that has the most significant distance to the nearest training data point of any class, since in general the more significant the margin, the lower the error of the classifier.

The optimal solution r* was obtained by minimizing the following cost function [35]:

Minimize

$$\frac{1}{2}\|w\|^2 + C\sum_{i=1}^{n}\xi_i,$$

subject to

$$y_i\left(w^T x_i + b\right)^3 \geq 1 - \xi_i, \quad \xi_i \geq 0, \tag{15}$$

where w^T, $x_i \in R^2$ and $b \in R^1$, $\|w\|^2 = w^T w$, C is the trade-off parameter between margin and error, ξ_i is the measure of training data, and y_i is the class label for the i^{th} sample. A third-degree polynomial kernel function was used with C = 0.5. 10-fold cross-validation was then applied to obtain classification accuracies. Due to dependency upon support vectors, equality is introduced in the constraint.

4.3. kNN

It is a non-parametric technique used for classification or regression in pattern recognition. It predicts test sample through *k* training samples, and after that classifies it based on largest category probability. Assume that there are j training categories, $C_1, C_2, C_3 \ldots C_j$ and N represent an entire number of training samples. Class Z represents the feature vector for all training samples. D_i is another neighbor existents in the training set, $y(D_i, C_j)$ represents whether D_i belongs to class C_j. $Sim(Z, D_i)$ denotes similarity function for D_i and Z. Thus, the probability density function for feature data Z, class C_j can be presented as in (16).

$$P(Z, C_j) = \sum_{D_i \varepsilon kNN} Sim\ (Z, D_i)\ .\ y(D_i, C_j), \tag{16}$$

where Sim (Z, D_i) was calculated using the Euclidean distance methods. The value of K is independent of number of classes. It means that K can be selected as any odd value like 3, 5, 7 and so on independent of how many classes need to be separated. The number of nearest neighbour was set to 5. For closest training data of class, the parameter k was considered 10 while 10-fold crossvalidation was performed for estimation of accuracies.

4.4. QDA

Quadratic discriminant analysis is similarly a robust classification method. It is a nonlinear technique for pattern classification. QDA models the likelihood of each class as a Gaussian distribution then use the posterior distributions to estimate the class for a given test point. The Gaussian parameters for each class can be estimated from training points using maximum likelihood estimation [36].

5. RESULTS

The experiment included two separate parts. The first part was an offline evaluation of EMG signals using Myo armband. In the second part, the subjects real-time performance was acessed to control a prosthetic arm. To achieve optimal accuracy, we compared four different classifiers as described in the previous section. At first, the classification accuracies of four classifiers were obtained using four features namely SM, σ, SSK, SK and their different combinations. These resulted in a maximum accuracy of 74.8% for healthy subjects and 50.2% for amputee subjects. These outcomes are not acceptable for control command generation so another set of six features namely RMS, WL, WAMP, SS, ZC, and MAV were used to check the classifier performance along with the signal mean. The obtained offline classification accuracy of each classifier for all healthy subjects and amputees using these six features are provided in Tables 3 and 4, respectively.

5.1. Real-time performance

The real-time classification was performed using kNN classifier and SM and WL features since this combination performed significantly better than others in an offline test. Performance parameters of real-time were measured using ST, CT and RA. ST represents the time required to produce the first correct prediction. It could also be seen as a response indicator for prosthesis control [37]. CT is the cumulative time to achieve ten correct predictions. RA represents the prediction accuracy from the first correct prediction until the end of the task. Fig. 4 shows the real-time performance metrics of fifteen healthy subjects.

Table 3. Offline classification accuracies of fifteen subjects using the second set of features namely RMS, WL, ZC, WAMP, MAV, and SS for four classifiers with the SM.

	WL				MAV				WAMP			
Subjects	**LDA**	**SVM**	**QDA**	**kNN**	**LDA**	**SVM**	**QDA**	**kNN**	**LDA**	**SVM**	**QDA**	**kNN**
S1	87.06	91.12	80.93	92.5	83.7	85.93	84.97	87.93	91.22	80.92	84.06	88.86
S2	93.92	88.22	84.86	93.9	85.06	79.86	85.06	89.1	88.42	80.92	83.22	83.33
S3	87.76	85.29	83.9	91.5	86.9	88.9	86.9	88.7	79.86	82.9	81.39	80.92
S4	95.2	93.7	95.12	95.8	91.22	91.9	91.22	81.63	88.9	80.92	83.22	79.94
S5	85.89	84.06	81.9	94.2	88.86	86.9	88.86	83.8	79.11	78.9	88.9	82.81
S6	80.86	83.9	79.37	94.6	84.06	84.37	84.06	90.12	86.9	88.9	85.93	85.66
S7	92	84.82	77.9	89.3	80.92	82.9	80.92	91.45	84.37	85.63	84.37	84.6
S8	76.63	74.92	76.39	85.7	83.22	81.39	83.22	88.54	82.9	88.9	85.93	82
S9	82.82	85.89	80.63	86	88.9	85.63	88.9	80.01	84.06	83.2	87.23	86.66
S10	86.9	80.98	79.37	85	85.93	84.37	85.93	82.89	80.92	77.91	88.34	84.59
S11	88.1	86.6	79.6	88	91.7	84.6	91.7	91.9	83.22	82.08	83.45	87.77
S12	88	89.6	86.9	89.45	86.5	91.9	86.5	78.73	81.85	83.76	79.67	81.99
S13	88.2	85.2	87.2	88.98	86.9	92.2	86.9	84.08	85.93	77.83	84.44	82.81
S14	82	80	93	91.98	86	88	86	86.81	79.99	85	86.31	85.93
S15	92	80.63	74.92	93.7	90	79.92	91.9	81.86	82.67	86.55	81.67	88.99
	ZC				**RMS**				**SS**			
	LDA	**SVM**	**QDA**	**kNN**	**LDA**	**SVM**	**QDA**	**kNN**	**LDA**	**SVM**	**QDA**	**kNN**
S1	80.86	87.65	78.76	88	92	88.49	93	91.98	84.99	88.04	85.31	86.93
S2	83.9	92	72.83	88.2	90.14	88.8	90.36	94.67	86	86.21	87	89.02
S3	79.37	84.82	88.04	92	83.42	75.92	78.22	78.33	94.7	94.43	93.7	88.81
S4	94.6	77.9	86.21	92	74.86	77.9	76.39	75.92	92.7	93.43	90.7	88.92
S5	81.9	89.3	87	92.31	93.9	88.92	89.22	93.94	93.31	93.7	94.02	94.88
S6	83.9	79.37	89.02	89.76	74.11	73.9	83.9	77.81	85.89	84.06	81.9	94.2
S7	80.93	80.63	83.34	83.11	81.9	83.9	80.93	80.66	80.86	83.9	79.37	94.6
S8	80.66	79.37	78.45	81.98	79.37	80.63	79.37	79.6	92	84.82	77.9	89.3
S9	89.91	79.6	74.67	85.44	87.9	86.9	88.86	89.76	76.63	74.92	76.39	85.7
S10	84.37	85	79.44	80.65	89.91	84.37	84.06	83.11	82.82	85.89	80.63	86
S11	78.7	82.9	85.31	86.28	85	82.9	80.92	81.98	86.9	80.98	79.37	85
S12	80.06	80.92	76.67	83.93	85.67	81.39	83.22	85.44	88.1	86.6	79.6	88
S13	86.9	81.98	88.9	91.9	90.94	85.63	88.9	80.65	93.86	91.9	93.86	92.7
S14	86.5	81.9	86.5	90.94	88.93	84.37	85.93	86.28	89.06	89.37	89.06	89.6
S15	86.9	92.2	86.9	86.98	81.7	84.6	84.01	83.93	85.06	79.86	85.06	83.57

Table 4. Offline classification accuracies of amputee subjects using RMS, WL, ZC, WAMP, MAV, and SS features.

Features	**A1**				**A2**			
	LDA	**SVM**	**QDA**	**kNN**	**LDA**	**SVM**	**QDA**	**kNN**
RMS	60.5	57.14	44.68	66.18	48.2	50.5	41.97	50.61
WL	55.75	67.3	56.3	56.87	50.97	47.77	54.89	54.49
ZC	42.45	51.65	53.14	56.65	56.18	53.21	40.45	52.94
WAMP	57.1	50.18	39.26	47.85	39.18	51.65	51.65	51.88
MAV	47.2	48.67	48.91	57.98	56.18	53.21	50.18	49.28
SS	46.88	52.91	55.1	58.28	49.03	51.52	40.05	42.65
	A3				**A4**			
	LDA	**SVM**	**QDA**	**kNN**	**LDA**	**SVM**	**QDA**	**kNN**
RMS	67	59.18	70.71	72.6	68.2	51.65	67.15	74.62
WL	65.5	56.18	64.62	70.07	69.5	50.18	63.4	59.6
ZC	68	49.03	64.71	68.6	69	40.05	58.8	69.6
WAMP	69.5	44.95	64.76	61.1	67	47.05	72.97	74.8
MAV	65	53.67	69.56	68.89	70	47.72	66.77	72.5
SS	72.7	44.18	70.61	63.84	68	51.93	60.69	74

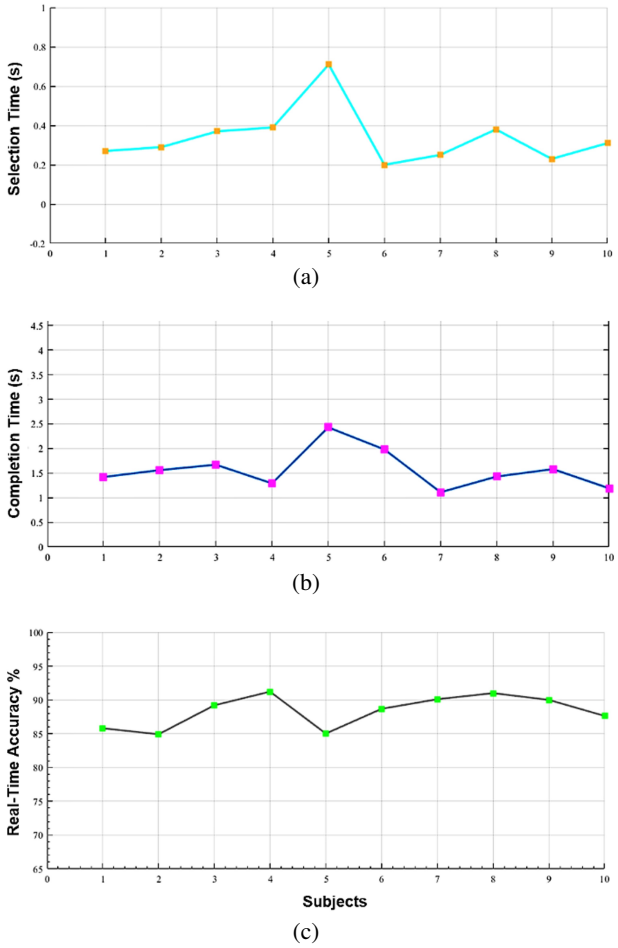

Fig. 4. Online performance metrics across ten healthy subjects for ten trails (a) ST (selection time), (b) CT (completion time), (c) RA (real-time accuracy).

5.2. Statistical analysis

Student's t-test was performed to establish the statistical significance of the obtained results. The confidence interval was set to 95% ($p < 0.05$). The quantitative comparison between healthy subjects and amputees was not possible due to a limited number of amputees. The *p*-value computed for the feature SM and WL was 0.0337 considering a 95% of a confidence interval. The results show that the features combination SM and WL with kNN classifier is statistically significant and performing better than the other features and classifiers.

6. DISCUSSION

The ultimate goal of this research is to develop a non-invasive and wearable transhumeral prosthetic arm. This arm is anticipated to be able to control at least six motions which are necessary to maintain minimum functionality of arms such as EE, EF, WP, WS, Hand Open (HO) and Hand Close (HC). Through this study, it has been confirmed that it is possible to obtain high classification accuracy for four different arm motion using a non-invasive and wearable sEMG armband. The prosthetic arm had an active elbow and wrist joint while the hand was a dummy version. The design and development of an under actuated three DoF prosthetic hand have been completed and is in integration phase with the current prosthetic arm. sEMG data from bicep and triceps of healthy and amputated subjects was also acquired for HO and HC motion. Due to the lack of available muscle in case of a transhumeral amputee, quality EMG muscles cannot be obtained for HO and HC motion. The obtained accuracy for the above-mentioned motion was around 50% which is not acceptable. In a previous study, the focus was to calculate the classification accuracy of eight arm motions and no motion class using sEMG data of transhumeral subjects. Five amputees took part in the experiment. Participants used mirror movements of their intact limb to aid in attempting movements with their residual limb. Ten different time-domain features were extracted from segmented raw sEMG signals. Mean Absolute Value (MAV), zero crossings (ZC), slope sign changes (SSC), Waveform length (WL), root mean square (RMS), mean absolute value slope (MAVS), Willison amplitude (WAMP), sample entropy (SampEn), 4th order auto-regressive model (AR) and 4th order cepstral analysis (CC). The highest classification accuracy for all DoF was obtained (93.0%) which is greater than the current literature as illustrated in Table 5, while the lowest (60.9%). The main reason for such deviated result is that one participant was subjected to amputation recently while the others had been amputated for over a year. The response of residual muscle gradually decreased and it became numb as more time passed. Indeed, the classification accuracy is 67.4%, 72.5%, 74.5%, and 76.3% respectively for a set of one, two, three and four time-domain features. The optimal feature set, which used MAV, CC, SampEn and WAMP, produced a classification accuracy (76.3%) that is almost equivalent to the accuracy using all ten time-

Table 5. Analysis of recent studies for upper limb prosthesis.

Year	Invasive/ Non-invasive	Features	Classifier	Accuracy	No. of Classes
2018 [3]	Non-invasive	10	DNN	93%	8
2020 [38]	Non-invasive	NA	RNN	79.7%	8
2018 [39]	Non-invasive	4	LDA	86.4	8
2018 [23]	Non invaisve	4	kNN,DNN	80.9	4

domain features (76.6%). Improvements in term of accuracy have been achieved while using one feature hence less computational time. The maximum accuracy and average accuracy of amputee subjects are higher than those reported by Gaudet *et al*. [3].

This research aimed to utilize an optimal feature and classifier in order to achieve the maximum classification accuracy for sEMG data and to control a prosthetic arm using non-invaisve sEMG signals acquired from biceps and triceps of healthy and amputated subjects. Unlike forearm; the arm, which is the part of the upper limb between the shoulder joint and the elbow joint, has minor muscle activity, and motions of the elbow joint and forearm twist cannot be predicted very easily from there. Therefore, non-invasive signal processing is a big challenge for above elbow amputation, but more experimentation and better feature and classifier selection may help in resolving such problems. Myo armband was used to acquire EMG signals. Experiments were performed both on healthy and amputated subjects. In case of amputated subjects, no partial elbow was present and actual wrist rotation was not performed. Instead, they just tried to move the residual limb that they thought could rotate wrist. Ten different features and their combinations were used with four classifiers LDA, QDA, SVM, and kNN. At first, classification accuracies of healthy and amputee subjects were obtained using SS, SV, SSK, and SK features and their combinations. The accuracies were mostly on the lower side. Then again classification accuracies for healthy and amputated subjects were obtained using RMS, WL, ZC, WAMP, MAV, and SS features. The classification accuracies of amputee subjects are lower than the acceptable range of 70%. This is because some added factors affect the classification accuracy for amputees such as a lesser available residual limb, condition of remnant arm muscles, fitting of prosthesis socket and time since the amputation. Also, the limitation of the sensor, some information is lost, as the operating frequency of the sensor is smaller than that of bandwidth of the electromyogram. The results can be implemented to a exoskeleton for real-time settings [40]. For future work, it is intended to use Brain-Computer Interface (BCI) to recognize hand open and hand close motions. As the key objective of this research is to provide a non-invaisve and wearable solution for transhumeral amputees, fNIRS or EEG might be considered for acquiring hand data.

7. CONCLUSION

The proposed research can be utilized for rehabilitation and training of transhumeral amputated subjects using EMG signals. It was found that feature WL performed significantly better ($p < 0.05$) than the other features and their combinations when fed to kNN classifier resulted in offline classification accuracies of 95.8% and 68.1%, and real-time classification accuracies of 91.9% and 60.11% for healthy and amputated subjects, respectively. The obtained results show that using appropriate features and classifier improves classification accuracies for control of prosthetic arm using EMG. Possible extension of this work could be to increase the number of classes, exploration of arm movement pattern for different age group and an increase in the number of amputated subjects.

REFERENCES

[1] A. H. Al-Timemy, R. N. Khushaba, G. Bugmann, and J. Escudero, "Improving the performance against force variation of EMG controlled multifunctional upper-limb prostheses for transradial amputees," *IEEE Transactions on Neural Systems and Rehabilitation Engineering*, vol. 24, no. 6, pp. 650-661, 2016.

[2] T. Lenzi, J. Lipsey, and J. W. Sensinger, "The RIC arm–a small anthropomorphic transhumeral prosthesis," *IEEE/ASME Transactions on Mechatronics*, vol. 21, no. 6, pp. 2660-2671, 2016.

[3] G. Gaudet, M. Raison, and S. Achiche, "Classification of upper limb phantom movements in transhumeral amputees using electromyographic and kinematic features," *Engineering Applications of Artificial Intelligence*, vol. 68, pp. 153-164, 2018.

[4] J.-W. Lee and G.-K. Lee, "Gait angle prediction for lower limb orthotics and prostheses using an EMG signal and neural networks," *International Journal of Control, Automation, and Systems*, vol. 3, no. 2, pp. 152-158, 2005.

[5] N. Naseer and K.-S. Hong, "Classification of functional near-infrared spectroscopy signals corresponding to the right-and left-wrist motor imagery for development of a brain–computer interface," *Neuroscience letters*, vol. 553, pp. 84-89, 2013.

[6] N. Naseer, K.-S. Hong, M. R. Bhutta, and M. J. Khan, "Improving classification accuracy of covert yes/no response decoding using support vector machines: An fNIRS study," *Proc. of International Conference on Robotics and Emerging Allied Technologies in Engineering (iCREATE)*, IEEE, pp. 6-9, 2014.

[7] K. Li, Y. Fang, Y. Zhou, and H. Liu, "Non-invasive stimulation-based tactile sensation for upper-extremity prosthesis: A review," *IEEE Sensors Journal*, vol. 17, no. 9, pp. 2625-2635, 2017.

[8] M. Jeong, H. Woo, and K. Kong, "A study on weight support and balance control method for assisting squat movement with a wearable robot, angel-suit," *International Journal of Control, Automation and Systems*, vol. 18, no. 1, pp. 114-123, 2020.

[9] O. W. Samuel, M. G. Asogbon, Y. Geng, A. H. Al-Timemy, S. Pirbhlal, N. Ji, S. Chen, P. Feng, and G. Li, "Intelligent EMG pattern recognition control method for upper-limb multifunctional prostheses: Advances, current challenges, and future prospects," *IEEE Access*, vol. 7, pp. 10150-10165, 2019.

[10] L. J. Hargrove, K. Englehart, and B. Hudgins, "A comparison of surface and intramuscular myoelectric signal classification," *IEEE Transactions on Biomedical Engineering*, vol. 54, no. 5, pp. 847-853, 2007.

[11] J. K. Lee, T. H. Jeon, and W. C. Jung, "Constraint-augmented Kalman filter for magnetometer-free 3D joint angle determination," *International Journal of Control, Automation and Systems*, vol. 18, no. 11, pp. 2929-2942, 2020.

[12] G. Yang, J. Deng, G. Pang, H. Zhang, J. Li, B. Deng, Z. Pang, J. Xu, M. Jiang, P. Liljeberg, H. Xie, and H. Yang, "An IoT-enabled stroke rehabilitation system based on smart wearable armband and machine learning," *IEEE Journal of Translational Engineering in Health and Medicine*, vol. 6, pp. 1-10, 2018.

[13] Y. Gu, D. Yang, Q. Huang, W. Yang, and H. Liu, "Robust EMG pattern recognition in the presence of confounding factors: Features, classifiers and adaptive learning," *Expert Systems with Applications*, vol. 96, pp. 208-217, 2018.

[14] A. Phinyomark, C. Limsakul, and P. Phukpattaranont, "A novel feature extraction for robust EMG pattern recognition," arXiv preprint, arXiv:0912.3973, 2009.

[15] A. J. Young, L. H. Smith, E. J. Rouse, and L. J. Hargrove, "Classification of simultaneous movements using surface EMG pattern recognition," *IEEE Transactions on Biomedical Engineering*, vol. 60, no. 5, pp. 1250-1258, 2013.

[16] E. Scheme and K. Englehart, "Electromyogram pattern recognition for control of powered upper-limb prostheses: state of the art and challenges for clinical use," *Journal of Rehabilitation Research & Development*, vol. 48, no. 6, 2011.

[17] D. A. Bennett, J. E. Mitchell, D. Truex, and M. Goldfarb, "Design of a myoelectric transhumeral prosthesis," *IEEE/ASME Transactions on Mechatronics*, vol. 21, no. 4, pp. 1868-1879, 2016.

[18] T. R. Farrell, "A comparison of the effects of electrode implantation and targeting on pattern classification accuracy for prosthesis control," *IEEE Transactions on Biomedical Engineering*, vol. 55, no. 9, pp. 2198-2211, 2008.

[19] C. L. Pulliam, J. M. Lambrecht, and R. F. Kirsch, "EMG-based neural network control of transhumeral prostheses," *Journal of Rehabilitation Research and Development*, vol. 48, no. 6, p. 739, 2011.

[20] P. F. Pasquina, M. Evangelista, A. J. Caravalho, J. Lockhart, S. Griffin, G. Nanos, P. McKey, M. Hansen, D. Ipsen, J. Vandersea, J. Butkus, M. Miller, I. Murphy, and D. Hankin, "First-in-man demonstration of a fully implanted myoelectric sensors system to control an advanced electromechanical prosthetic hand," *Journal of Neuroscience Methods*, vol. 244, pp. 85-93, 2015.

[21] P. Geethanjali, "Myoelectric control of prosthetic hands: State-of-the-art review," *Medical Devices (Auckland)*, vol. 9, p. 247-255, 2016.

[22] M. S. Fifer, H. Hotson, B. A. Wester, D. P. McMullen, Y. Wang, M. S. Johannes, K. D. Katyal, J. B. Helder, M. P. Para, R. J. Vogelstein, W. S. Anderson, N. V. Thakor, and N. E. Crone, "Simultaneous neural control of simple reaching and grasping with the modular prosthetic limb using intracranial EEG," *IEEE Transactions on Neural Systems and Rehabilitation Engineering*, vol. 22, no. 3, pp. 695-705, 2014.

[23] D. Bandara, J. Arata, and K. Kiguchi, "Towards control of a transhumeral prosthesis with EEG signals," *Bioengineering*, vol. 5, no. 2, p. 26, 2018.

[24] T. Sittiwanchai, I. Nakayama, S. Inoue, and J. Kobayashi, "Transhumeral prosthesis prototype with 3D printing and sEMG-based elbow joint control method," *Proceedings of the International Conference on Advanced Mechatronic Systems*, IEEE, pp. 227-231, 2014.

[25] M. E. Benalcázar, A. G. Jaramillo, A. Zea, A. Páez, and V. H. Andaluz, "Hand gesture recognition using machine learning and the Myo armband," *Proc. of 25th European Signal Processing Conference (EUSIPCO)*, IEEE, pp. 1040-1044, 2017.

[26] N. Y. Sattar, U. A. Syed, S. Muhammad, and Z. Kausar, "Real-time EMG signal processing with implementation of PID control for upper-limb prosthesis," *Proc. of IEEE/ASME International Conference on Advanced Intelligent Mechatronics (AIM)*, IEEE, pp. 120-125, 2019.

[27] U. A. Syed, Z. Kausar, and N. Y. Sattar, "Control of a prosthetic arm using fNIRS, a neural-machine interface," *Data Acquisition-Recent Advances and Applications in Biomedical Engineering: IntechOpen*, 2020.

[28] F. Liu, Z. Gao, C. Yang, and R. Ma, "Extended Kalman filters for continuous-time nonlinear fractional-order systems involving correlated and uncorrelated process and measurement noises," *International Journal of Control, Automation and Systems*, vol. 18, pp. 2229-2241, 2020.

[29] M. Rahmani and M. H. Rahman, "Adaptive neural network fast fractional sliding mode control of a 7-DoF exoskeleton robot," *International Journal of Control, Automation and Systems*, vol. 18, no. 1, pp. 124-133, 2020.

[30] X. Zhang, X. Wang, B. Wang, T. Sugi, and M. Nakamura, "Meal assistance system operated by electromyogram (EMG) signals: Movement onset detection with adaptive threshold," *International Journal of Control, Automation and Systems*, vol. 8, no. 2, pp. 392-397, 2010.

[31] B. Wang, Z. Li, W. Ye, and Q. Xie, "Development of human-machine interface for teleoperation of a mobile manipulator," *International Journal of Control, Automation and Systems*, vol. 10, no. 6, pp. 1225-1231, 2012.

[32] K.-S. Hong and M. J. Khan, "Hybrid brain–computer interface techniques for improved classification accuracy and increased number of commands: A review," *Frontiers in Neurorobotics*, vol. 11, p. 35, 2017.

[33] K.-S. Hong, N. Naseer, and Y.-H. Kim, "Classification of prefrontal and motor cortex signals for three-class fNIRS–BCI," *Neuroscience Letters*, vol. 587, pp. 87-92, 2015.

[34] S. Belkacem, F. Naceri, and R. Abdessemed, "Improvement in DTC-SVM of AC drives using a new robust adaptive control algorithm," *International Journal of Control, Automation and Systems*, vol. 9, no. 2, pp. 267-275, 2011.

[35] S. S. Esfahlani, B. Muresan, A. Sanaei, and G. Wilson, "Validity of the Kinect and Myo armband in a serious game for assessing upper limb movement," *Entertainment Computing*, vol. 27, p. 150-156, 2018.

[36] K. T. Reilly, C. Mercier, M. H. Schieber, and A. Sirigu, "Persistent hand motor commands in the amputees' brain," *Brain*, vol. 129, no. 8, pp. 2211-2223, 2006.

[37] T. A. Kuiken, G. Li, B. A. Lock, R. D. Lipschutz, L. A. Miller, K. A. Stubblefield, and K. B. Englehart, "Targeted muscle reinnervation for real-time myoelectric control of multifunction artificial arms," *JAMA*, vol. 301, no. 6, pp. 619-628, 2009.

[38] O. Barron, M. Raison, G. Gaudet, and S. Achiche, "Recurrent neural network for electromyographic gesture recognition in transhumeral amputees," *Applied Soft Computing*, vol. 96, 106616, 2020.

[39] N. Jarrassé, E. de Montalivet, F. Richer, C. Nicol, A. Touillet, N. Martinet, J. Paysant, and J. B. de Graaf, "Phantom-mobility-based prosthesis control in transhumeral amputees without surgical reinnervation: A preliminary study," *Frontiers in Bioengineering and Biotechnology*, vol. 6, 2018.

[40] M. Rahmani, M. H. Rahman, and J. Ghommam, "A 7-DoF upper limb exoskeleton robot control using a new robust hybrid controller," *International Journal of Control, Automation and Systems*, vol. 17, no. 4, pp. 986-994, 2019.

Neelum Yousaf Sattar is pursuing her Ph.D. in mechatronics engineering. She received her M.S. degree in mechatronics engineering from Air University in 2015. Her research interests include Control theory and application, robotics and automation systems and bio-mechatronics.

Zareena Kausar received her Ph.D. degree in engineering from University of Auckland in 2013. Her research interests include dynamics modeling of mechatronics systems, non-linear control, biomechatronics, robotics, mechatronics system design.

Syed Ali Usama received his M.S. degree in mechatronics from the Air University, Islamabad, Pakistan in 2020. He is currently a Lab Engineer in teh Department of Mechatronics and Biomedical Engineering, Air University. His research areas include human-machine interface, assistive robotics, intelligent control, artificial intelligence, biomechatronic and neuroscience.

Umer Farooq has received his M.S. degree in computer engineering from LUMS. Currently he is working as a Lecturer in the Department of Mechatronics Engineering at Air University since 2013 with a keen interest in Industrial/Commercial Problem Solving & Research opportunities, and aspires to bridge the gap between Academia & Industry.

Umar Shahbaz Khan completed his Ph.D. in electrical engineering from University of Liverpool, UK in 2010. Currently he is working as an Assistant professor at the Department of Mechatronics Engineering, National University of Sciences and Technology and his research interests include electrical systems manufacturing. He is also the project director of National Centre of Robotics and Automation.